

Non-adiabatic Oscillations of Red Giants

D.R. Xiong¹ & L. Deng²

¹*Purple Mountain Observatory, Chinese Academy of Sciences, Nanjing 210008; Xiongdr@pmo.ac.cn*

²*National Astronomical Observatories, Chinese Academy of Sciences, Beijing 100012; licai@bao.ac.cn*

22 November 2021

ABSTRACT

Using our non-local time-dependent theory of convection, the linear non-adiabatic oscillations of 10 evolutionary model series with masses of 1–3 M_{\odot} are calculated. The results show that there is a red giant instability strip in the lower temperature side of the Hertzsprung-Russel (HR) diagram which goes along the sequences of the red giant branch (RGB) and the asymptotic giant branch (AGB). For red giants of lower luminosities, pulsation instability are found at high order overtones, the lower order modes from the fundamental to the second overtone are stable. Towards higher luminosity and lower effective temperature, instability moves to lower order modes, and the amplitude growth rate of oscillations also grows. At the high luminosity end of the strip, the fundamental and the first overtone become unstable, while all the modes above the 4th order become stable. The excitation mechanism have been studied in detail. It is found that turbulent pressure plays a key role for exciting of red variables. The frozen convective approximation is unavailable for the low temperature stars with extended convective envelopes. In any case, this approximation can explain neither the red edge of the Cepheid instability strip, nor the blue edge of the pulsating red giant instability strip. An analytic expression of a pulsation constant as a function of stellar mass, luminosity and effective temperature is presented from this work.

Key words: convection—stars:variables—stars:late-type—stars:evolution

1 INTRODUCTION

The Mira type variables are among the most luminous stars in a star cluster, and they possess very large light amplitudes therefore they are the first variable stars ever discovered. The red variables, however, are not yet understood well. According to Wood (2000) "red giant stars are probably the least understood of all variable stars". It was suspected long time ago that all red stars are variables. Eggen (1969) pointed out, for instance, that all old disc population red giants with $(R-I)_0 \geq 1.0$ are variables. A few year later, he shifted the blue edge of that instability area to $(R-I)_0 \approx 0.9$ (Eggen 1973). The visual amplitudes of red variables have vary large ranges, from 0.01 to 10 magnitudes, and the typical time scales (periods) goes from several to a few hundred days. Classification of these red variables based on period, luminosity and population data were made by Eggen (1972a,b, 1973a,b, 1975, 1977). By photometric and spectroscopic observations of 187 G & K type giants, Henry et al. (2000) showed that all K5-M0 type giants are variables, and they further claimed that the variations of red giants with spectral type later than K2 are resulted from pulsation. Towards lower effective temperature and higher luminosity, the light amplitude tends to increase. In fact, these stars are located either in the upper part of RGB or

on AGB. It is identified by Percy et al. (1998, 2001, 2003) that these stars are actually pulsating from the fundamental up to the 3rd overtone. It is also found that there are variables with rather short periods from several hours to ~ 2 days and small amplitudes from several to 20 percents of a magnitude on the lower RGB of globular clusters (Yao & Qin 1993, Yao, Zhang & Qin 1993). By analyzing the 38.5 day photometric data acquired by HST for 47 Tuc, Edmonds & Gilliland (1996) discovered a mount of small amplitude K type variables on RGB, whose periods go from 2 to 4 days and the amplitudes only measure 5–15mmag. On the V–(B–V) color magnitude diagram (CMD) of 47 Tuc, one group of these variables gathers near the red edge of the horizontal branch (HB), while another stays on the RGB and the bottom of the AGB about 1 magnitude brighter than the HB of the cluster.

The observational studies of red giant variables gains are advanced by the variable star survey programs and gravitational lensing survey projects started in recent years, such as the *Long-Term Photometry of Variables* (Jorissen et al. 1997), the *All Sky Automated Survey* (Pojmanski 2002) and the *Northern Sky Survey* (Wozniak et al. 2004) etc., especially, MACHO (Alcock et al. 2000, Wood et al. 1999, Schultheis 2004), OGLE (Kiss & Bedding 2003, 2004, Wrag et al. 2004, Soszyński et al. 2004), EROS (Cioni et al. 2001)

and MOA (Bond et al. 2001, Noda et al. 2002) have accumulated a huge time sequenced stellar photometric data set that is suitable for searching of variable stars. Wood (2000) found 5 distinct period-luminosity sequences (A, B, C, D & E, as he defined) in the K - $\log P$ diagram based on his analysis of the MACHO near infrared J & K broadband photometry data in the half square degree field of the LMC bar from. In that, the sequence C was the Mira variables identified as the fundamental radial mode. The stars on the sequence B would be known as semi-regular (SR) variables and A are of very low amplitude as small amplitude red variables (SARVs). The sequence B and A correspond to pulsation in first-third overtones (Wood, 2000). Such result is later confirmed independently by OGLE observations (Kiss & Bedding 2003, 2004). It is further pointed out by Soszyński et al. (2004) that the OGLE small amplitude variable red giants (OSARGs) and the long period variables (LPVs) are two distinct types of pulsating red variables.

The excitation mechanism of the pulsating red variables are far from fully understood, the principal barrier is that there is not yet a perfect time-dependent convection theory that can handle the coupling between convection and oscillations. Most of the studies either simply neglected the coupling between convection and oscillations, such as Ostlie & Cox (1986) and Gong et al. (1995), or over-simplified it, such as Cox & Ostlie (1991), Fox & Wood (1982). The most careful treatment of the coupling between convection and oscillations comes from Balmforth (1992) and Xiong, Deng & Cheng (1998), with the former study applied Gough's (1977) non-local time-dependent mixing-length theory of convection, while the later one adopted Xiong's (1989a) time-dependent statistical theory of convection. In our case, Xiong, Deng & Cheng (1998) studied the oscillations of Mira variables. The results show that for the luminous red giants, the oscillations tend to happen in the fundamental and low overtones whose amplitude growth rate is very large, i.e. the amplitude gets doubled within a few, or sometimes even within a single period. All the overtones above 4th order are stable. For intermediate and low luminosity red giants, however, the fundamental mode and the 1st overtone are stable while being unstable at modes above the 2nd overtone (Xiong & Deng 2001a). These SARVs have rather small amplitude growth rates, being almost neutrally stable, therefore special care is needed to handle convection in this situation. The goal of the present work is to deliver a thorough study of pulsation stability in stars with intermediate- and low-luminosity on the RGB and AGB. The second section describes the refinement and specification of the convection theory for the current work, and the third section presents the results of linear non-adiabatic computations. The excitation mechanism for the red variables is discussed in section 4. The conclusions of this work and discussions are given in the last section.

2 THE FUNDAMENTAL EQUATIONS

Stars near the Hayashi limit (RGB and AGB) all have very deep convective envelope. Instead of the κ -mechanism operating in the hot and warm stars, the coupling between convection and oscillations will be the primary mechanism of excitation and damping for these cold stars. The main

difficulty prevent us from understanding the oscillations of such stars has been the lack of a perfect convection theory. Being distinct from the pulsational properties in the even cooler and brighter long period variables, the pulsation amplitudes of the intermediate and low luminosity red giants should be very small if any unstable p-mode oscillations can be excited. This fact actually requires very careful treatment of the coupling between convection and oscillations, therefore makes the problem especially challenging.

Convection transfers energy and momentum inside stars, and causes mixing of matters. A star, as a thermodynamic system, can also be regarded as a heating (or cooling) machine when considering its thermodynamic behavior. Based on its nature and mechanism of working, the coupling between convection and oscillations can be divided into two types as the following:

(i) The thermodynamic coupling between convection and oscillations, whose mechanism is to adjust the temperature and pressure of stellar material through its energy transfer function, therefore affects the pulsational stability of the star. Its general effect is damping. The thermodynamic coupling is the major reason for the existence of the red edge of the Cepheid instability strip (including RR Lyrae and δ Scuti) in the HRD (Xiong, Cheng & Deng 1998, Xiong & Deng 2001a).

(ii) The dynamic coupling between convection and oscillations, whose mechanism is to trigger momentum transfer within a star, i.e. to affect the stability through turbulent pressure and turbulent viscosity. Turbulent viscosity is always a damping, while turbulent pressure is generally a excitation for oscillations. Such coupling plays a key role in exciting the red pulsating variable stars (Xiong, Deng & Cheng 1998).

The relative contributions of convective energy transfer, turbulent pressure and turbulent viscosity to the instability of low temperature stars change with temperature, luminosity and pulsating mode of the stars, and this fact can be used to explain the complex behaviors of pulsation instability among these stars having extended convective envelopes. It is therefore quite easy to understand such questions as follows: Why does the Cepheid instability strip have a red edge? Why do the long period variables exist outside the Cepheid instability strip? What makes the luminous red variable stars to have higher amplitudes and to pulsate at the fundamental and lower order overtones than other stars, and what is the reason for the decreasing of amplitudes in the red variables with decreasing luminosity and eventually becoming pulsationally stable?

The main challenge in handling the coupling between convection and oscillations is the requirement of a time-dependent theory of convection. Owing to the huge scale of stars, stellar convection is generally fully developed turbulence which is still not yet understood satisfactorily. The main difficulty is due to the nonlinearity and the non-locality of hydrodynamics. Compared to the thermodynamic coupling between convection and oscillations, the dynamical coupling is even more difficult to deal with, for the anisotropic of stellar convection. The convection theory applied in this work is a time-dependent one. Neglecting stellar rotation and magnetic field, the full set of equations used in

the calculations of stellar convective envelope structure and radial oscillations is the following,

$$\frac{\partial r^3}{\partial M_r} = \frac{3}{4\pi\bar{\rho}} \quad (1)$$

$$\begin{aligned} \frac{D\bar{u}_r}{DM_r} &= -4\pi r^2 \frac{\partial}{\partial M_r} (\bar{\rho} + \bar{\rho}\chi^2) \\ &\quad - \frac{1}{r} \frac{\partial}{\partial M_r} (4\pi r^3 \bar{\rho}\Pi^{11}) - \frac{GM_r}{r^2}, \end{aligned} \quad (2)$$

$$\begin{aligned} C_P \frac{D\bar{T}}{Dt} + \frac{3}{2} \frac{D\chi^2}{Dt} - \frac{B}{\bar{\rho}} \frac{D\bar{P}}{Dt} - \frac{\chi^2}{\bar{\rho}} \frac{D\bar{\rho}}{Dt} = \\ - \frac{\partial}{\partial M_r} (L_r + L_c + L_t), \end{aligned} \quad (3)$$

$$L_r = - \frac{16\pi^2 a c r^4}{3\kappa} \frac{\partial \bar{T}^4}{\partial M_r}, \quad (4)$$

$$\begin{aligned} \frac{3}{2} \frac{D\chi^2}{Dt} - \frac{\chi^2}{\bar{\rho}} \frac{D\bar{\rho}}{Dt} + 4\pi\bar{\rho}r^3\Pi^{11} \frac{\partial}{\partial M_r} \left(\frac{\bar{u}_r}{r} \right) \\ - BV \left(\frac{D\bar{u}_r}{Dt} + \frac{GM_r}{r^2} \right) + \frac{\partial}{\partial M_r} (4\pi r^2 \overline{\bar{\rho}u_r w_i' w_i'/2}) \\ = - 1.56 \frac{GM_r \bar{\rho} \chi^3}{c_1 r^2 \bar{P}} \end{aligned} \quad (5)$$

$$\begin{aligned} \frac{DZ}{Dt} + 2Z \left\{ \left[1 - B + \left(\frac{\partial \ln C_P}{\partial \ln T} \right)_T \right] \frac{D \ln \bar{T}}{Dt} \right. \\ \left. + \left[(B-1) \nabla_{ad} + \left(\frac{\partial \ln C_P}{\partial \ln P} \right)_T \right] \frac{D \ln \bar{P}}{Dt} \right\}, \\ + 8\pi r^2 \bar{\rho} V \left(\frac{\partial \ln \bar{T}}{\partial M_r} - \nabla_{ad} \frac{\partial \ln \bar{P}}{\partial M_r} \right) \\ + \frac{1}{\bar{\rho} \bar{C}_P^2} \frac{\partial}{\partial M_r} \left[4\pi r^2 \bar{\rho}^2 \bar{C}_P^2 u_r' \overline{\left(\frac{T'}{\bar{T}} \right)^2} \right] \\ = - 1.56 \frac{GM_r \bar{\rho}}{c_1 r^2 \bar{P}} (\chi + \chi_c) Z, \end{aligned} \quad (6)$$

$$\begin{aligned} \frac{DV}{Dt} + V \left\{ 4\pi r^2 \bar{\rho} \frac{\partial \bar{u}_r}{\partial M_r} + \left[1 - B + \left(\frac{\partial \ln C_P}{\partial \ln T} \right)_P \right] \frac{D \ln \bar{T}}{Dt} \right. \\ \left. + \left[(B-1) \nabla_{ad} + \left(\frac{\partial \ln C_P}{\partial \ln P} \right)_T \right] \frac{D \ln \bar{P}}{Dt} \right\} \\ - BZ \left(\frac{D\bar{u}_r}{Dt} + \frac{GM_r}{r^2} \right) + 4\pi r^2 \bar{\rho} \chi^2 \left(\frac{\partial \ln \bar{T}}{\partial M_r} - \nabla_{ad} \frac{\partial \ln \bar{P}}{\partial M_r} \right) \\ + \frac{1}{C_P} \frac{\partial}{\partial M_r} \left(4\pi r^2 \bar{\rho} C_P u_r' \overline{\frac{T'}{\bar{T}}} \right) \\ = - 0.78 \frac{GM_r \bar{\rho}}{c_1 r^2 \bar{P}} (3\chi + \chi_c) V, \end{aligned} \quad (7)$$

$$\begin{aligned} \frac{\Pi^{11}}{Dt} + \frac{4}{3} \pi r^3 \bar{\rho} \chi^2 \frac{\partial}{\partial M_r} \left(\frac{\bar{u}_r}{r} \right) \\ + \frac{4}{3} \Pi^{11} \left[4\pi r^3 \bar{\rho} \frac{\partial}{\partial M_r} \left(\frac{\bar{u}_r}{r} \right) + \frac{3\bar{u}_r}{2r} \right] \\ - \frac{4}{3} BV \left(\frac{D\bar{u}_r}{Dt} + \frac{GM_r}{r^2} \right) + \frac{\partial}{\partial M_r} (4\pi r^2 \overline{\bar{\rho}u_r \Pi^{11}}) \\ = - \frac{4}{3} \frac{0.78(1+c_3)GM_r \bar{\rho}}{c_1 r^2 \bar{P}} \chi \Pi^{11}, \end{aligned} \quad (8)$$

where r is the radius, M_r is the mass within the sphere of radius r , u_r is the radial component of the velocity, T and P are respectively the regular notations for density, temperature and pressure (including radiative), χ is the opacity, C_P is the specific heat at constant pressure, $B = -(\partial \ln \rho / \partial \ln T)_P$ is the expansion coefficient of gas. Our formulism of stellar convection is a statistical theory of correlation functions based on hydrodynamics and the theory of turbulence, χ^2 and Π^{ij} are respectively the isotropic and the anisotropic components of the auto-correlation of turbulent velocity w^i , therefore we have,

$$\overline{w^i w'^j} = g^{ij} \chi^2 + \Pi^{ij}, \quad (9)$$

Z and V are respectively the auto-correlation of turbulent temperature fluctuation T'/\bar{T} and the cross-correlation of radial turbulent velocity and temperature, defined as,

$$Z = \overline{\left(\frac{T'}{\bar{T}} \right)^2}, \quad (10)$$

$$V = \overline{w_r' \frac{T'}{\bar{T}}}. \quad (11)$$

In our equations, all the quantities with a prim are the turbulent fluctuations, while those with a bar are statistical averages of the corresponding quantities.

Eqs. (1)–(8) are derived based the equations of hydrodynamics and the theory of turbulence, where Eqs. (1)–(4) are the normal equations for stellar structure, being different from the traditional expressions only by having the turbulent Renold's stress (turbulent pressure and viscosity) included in eq. (2) and having both the turbulent thermal convective flux $L_c = 4\pi r^2 \overline{\bar{\rho} C_P \bar{T} V}$ and the turbulent kinetic energy flux $L_t = 4\pi r^2 \overline{\bar{\rho} u_r' w_i' w_i'/2}$ included in eq. (3). As a result of this consideration, the correlations of turbulent convection also show up eqs. (2) and (3). Eqs. (5)–(8) are a set of dynamical equations of turbulent convection under non-local theoretical frame. Owing to the fact that the equations of stellar structure include the convective quantities and the stellar structural quantities, $\bar{\rho}$, \bar{P} and \bar{T} (and \bar{u}_r as well) enter the dynamical equations of turbulent correlations of eqs. (5)–(8), it makes these equations coupled with each other, therefore eqs. (1)–(8) formed a complete set of equations for the structure and oscillations of stellar envelope at spherical symmetry condition (of course without rotation and magnetic field, as we assumed at the beginning). In the frame work of the local theory, stellar convection is handled with a set of algebraic equations, while under non-local expressions it is dealt with by a set a differential (or integral) equations. In nature, all fluid motions are in fact non-local, the local convection approximation is good only at a limited local region (such as the interior zones far away from the boundaries of a convective zone). The local theory has no chance to be right when considering a whole convective region as an entity. This is especially true near the boundaries and the overshooting zones where the local approximation should be completely lifted, and in this context, one has to use a non-local theory. Our non-local theory of stellar convection is a statistical theory of turbulent correlations derived from hydrodynamics and the theory of turbulence, its physical picture is very clear. Eqs. (5)–(8) describe a statistical equilibrium of turbulent correlations. Turbulence gains energy from buoyant force and the average of motion

of fluid, this process happens in the low wave number region of the turbulent spectrum. Due to the non-linearity and interactions of fluid motion, turbulent energy is cascaded towards higher wave numbers from lower wave numbers, and is turned into thermal energy by molecular viscosity and is eventually completely dissipated. The right hand side terms including the convection parameter c_1 in eqs. (5)–(8) represent here the turbulent viscous dissipation. following the turbulence theory the dissipation rate of turbulent kinetic energy $\bar{\rho}\epsilon$ can be expressed as follows (Hinze 1975),

$$\epsilon = 2\eta_e k_e \chi^3, \quad (12)$$

where $k_e = \sqrt{3}k_{e1} = \sqrt{3}/l_{e1}$ is the wave number of the energy-containing eddies. It is assumed in this work that l_{e1} is proportional to the local pressure scale height, i.e.,

$$l_{e1} = c_1 H_P = c_1 \frac{r^2 P}{GM_r \bar{\rho}}. \quad (13)$$

The third order correlations in eqs. (5)–(8) correspond to the non-local convective diffusion. The third order correlation term in eq. (5), for example, is just the turbulent kinetic energy flux. A gradient type of diffusion approximation for the third order correlations is adopted in our theory of non-local convection. Taking the third order correlation for turbulent velocity as a instance, we have,

$$L_t = 4\pi r^2 \overline{\bar{\rho} u'_r w'_i w'^i / 2} = -6\pi r^2 \bar{\rho} \chi \Lambda \frac{\partial \chi^2}{\partial r}, \quad (14)$$

where Λ is the diffusion length assumed to be proportional to the local pressure scale height,

$$\Lambda = \frac{\sqrt{3}}{4} c_2 H_P = \frac{\sqrt{3}}{4} c_2 \frac{r^2 \bar{P}}{GM_r \bar{\rho}}, \quad (15)$$

where c_2 is another convective parameter that is linked to the non-local turbulent diffusion process.

Putting eq. (15) into eq. (14), L_t can be rewritten as,

$$L_t = -\frac{3}{2} Q \frac{\partial \chi^2}{\partial M_r}, \quad (16)$$

where,

$$Q = \frac{4\sqrt{3}\pi^2 c_2 r^6 \bar{\rho} \bar{P} \chi}{GM_r}. \quad (17)$$

Following similar operations, the remaining third order correlations in eqs. (6)–(8) can be given as,

$$4\pi r^2 \bar{\rho}^2 C_P^2 u'_r \left(\frac{T'}{\bar{T}} \right)^2 = -\bar{\rho} C_P^2 Q \frac{\partial Z}{\partial M}, \quad (18)$$

$$4\pi r^2 \bar{\rho} C_P u'^2_r \left(\frac{T'}{\bar{T}} \right) = -C_P Q \frac{\partial V}{\partial M_r}, \quad (19)$$

$$4\pi r^2 \bar{\rho} u'_r \Pi^{11} = -Q \frac{\partial \Pi^{11}}{\partial M_r}. \quad (20)$$

As described above, in the static station convection gains energy from buoyant force, therefore the initial convective motion is in radial direction. However, due to the continuity of fluid motion and the non-linear interactions among the turbulent eddies, a part of the initial turbulent kinetic energy will be converted into the horizontal directions. It is known from the theory of turbulence that the correlation of turbulent pressure and velocity gradient tends to make turbulence isotropic (Rotta 1951). The convection parameter c_3 in eq. (8) is introduced to describe the tendency of

restoring the isotropy. The larger c_3 , the stronger the restoring force and the turbulence is therefore more isotropic. Therefore, the convection parameter c_3 can be regarded as the parameter for the degree of isotropy of turbulence. In the convectively unstable zone, the ratio of the radial component of turbulence (w'_r) and the horizontal one (w'_h) is $\frac{\overline{w_r'^2}}{\overline{w_h'^2}} \approx (3 + c_3) / 2c_3$ (Deng & Xiong 2006).

Eqs. (1)–(8) are a completed set of dynamical equations of stellar envelope structure, which can be used to construct the equilibrium envelope model and to calculate the radial oscillations. When setting all the terms involving time derivatives and velocity \bar{u}_r in these equations to be zero, we will get the equations for equilibrium model. When a star does small amplitudes oscillations around the equilibrium, all the quantities can be made to be the sum of the equilibrium values and the perturbation (oscillations), then a Tyler expansion around the equilibrium can be applied. By conserving only the linear terms and neglecting all terms over the first order, we will get the equations of linear non-adiabatic oscillations. Details on the equations for equilibrium model and linear pulsation, and the method for solving these equations are not given here, for those who are interested in that, our previous work is referred (Xiong & Deng 2001b, Xiong, Deng & Cheng 1998). It needs to be noticed that we assumed quasi-isotropy for turbulent convection in our previous work. In the current, turbulent convection is more carefully handled, with anisotropy of turbulence included, i.e. a equation designated to the anisotropy of turbulent convection (8) is now added to the equations for both the equilibrium model and oscillations.

3 NUMERICAL RESULTS OF LINEAR NON-ADIABATIC OSCILLATIONS FOR RED GIANTS

Making use of the equations introduced in the previous section, the linear non-adiabatic oscillations of 10 sequences of evolutionary models with masses $M = 1, 1.2, 1.4, 1.6, 1.8, 2.0, 2.25, 2.5 \& 2.75 M_\odot$ are calculated. The chemical composition of all these models is solar, $X = 0.70$ and $Z = 0.02$. The evolutionary tracks are made using Padova code (Bressan, et al. 1993). For selected stellar models along the tracks with given luminosity and effective temperature, the corresponding non-local convective models of equilibrium envelope are constructed, then linear non-adiabatic oscillations for the fundamental through 11th overtones are further calculated. Special care is taken when handling thermodynamical and dynamical coupling between convection and oscillation as describe in detail in the previous section. Table 1 gives, as an example, the amplitude growth rate $r = -2\pi\omega_i/\omega_r$ of linear non-adiabatic oscillations for one of the evolutionary model with mass $M = 1.0 M_\odot$, where ω_i and ω_r are respectively the imaginary and the real component of the complex frequency of oscillations $\omega = i\omega_i + \omega_r$.

The equation of state adopted in this work is a simplified MHD expression. The main simplification made here is that a helium atom is still considered as a quasi-hydrogen atom, which makes the calculation for the energy levels of helium atomic far easier. For the first ionized helium atoms or the high level excitation states of neutral helium atoms,

Table 1. Amplitude growth rates for a set of evolutionary models of star with $1M_{\odot}$

No	Log Te	Log L	RATE0	RATE1	RATE2	RATE3	RATE4	RATE5	RATE6	RATE7	RATE8
1	3.7535	-0.1591	-0.15E-8	-0.16E-7	-0.82E-7	-0.31E-6	-0.93E-6	-0.22E-5	-0.48E-5	-0.97E-5	-0.19E-4
2	3.7460	-0.2022	-0.12E-8	-0.12E-7	-0.64E-7	-0.24E-6	-0.73E-6	-0.18E-5	-0.39E-5	-0.79E-5	-0.16E-4
3	3.7365	-0.2256	-0.81E-9	-0.10E-7	-0.53E-7	-0.20E-6	-0.62E-6	-0.15E-5	-0.33E-5	-0.69E-5	-0.13E-4
4	3.7264	-0.2407	-0.13E-8	-0.82E-8	-0.46E-7	-0.18E-6	-0.54E-6	-0.14E-5	-0.30E-5	-0.62E-5	-0.12E-4
5	3.7550	0.3154	-0.17E-7	-0.19E-6	-0.93E-6	-0.33E-5	-0.89E-5	-0.19E-4	-0.40E-4	-0.75E-4	-0.93E-4
6	3.7452	0.1800	-0.57E-8	-0.72E-7	-0.39E-6	-0.14E-5	-0.41E-5	-0.94E-5	-0.20E-4	-0.42E-4	-0.64E-4
7	3.7500	0.0048	-0.33E-8	-0.32E-7	-0.17E-6	-0.63E-6	-0.19E-5	-0.44E-5	-0.92E-5	-0.19E-4	-0.36E-4
8	3.7412	0.3459	-0.12E-7	-0.17E-6	-0.93E-6	-0.34E-5	-0.90E-5	-0.20E-4	-0.45E-4	-0.79E-4	-0.80E-4
9	3.7353	0.3515	-0.10E-7	-0.16E-6	-0.89E-6	-0.32E-5	-0.87E-5	-0.20E-4	-0.45E-4	-0.77E-4	-0.74E-4
10	3.7307	0.3554	-0.89E-8	-0.15E-6	-0.86E-6	-0.32E-5	-0.85E-5	-0.20E-4	-0.46E-4	-0.78E-4	-0.73E-4
11	3.7268	0.3548	-0.48E-8	-0.14E-6	-0.81E-6	-0.30E-5	-0.81E-5	-0.19E-4	-0.44E-4	-0.72E-4	-0.63E-4
12	3.7217	0.3520	-0.56E-8	-0.12E-6	-0.75E-6	-0.28E-5	-0.76E-5	-0.18E-4	-0.42E-4	-0.68E-4	-0.58E-4
13	3.7156	0.3514	-0.47E-8	-0.11E-6	-0.69E-6	-0.26E-5	-0.71E-5	-0.18E-4	-0.41E-4	-0.64E-4	-0.52E-4
14	3.7107	0.3492	-0.48E-8	-0.98E-7	-0.63E-6	-0.24E-5	-0.67E-5	-0.17E-4	-0.39E-4	-0.60E-4	-0.49E-4
15	3.7067	0.3502	-0.43E-8	-0.99E-7	-0.63E-6	-0.24E-5	-0.65E-5	-0.16E-4	-0.35E-4	-0.48E-4	-0.24E-4
16	3.7009	0.3512	-0.33E-8	-0.99E-7	-0.64E-6	-0.24E-5	-0.64E-5	-0.15E-4	-0.32E-4	-0.36E-4	0.42E-5
17	3.6962	0.3590	-0.31E-8	-0.10E-6	-0.66E-6	-0.24E-5	-0.64E-5	-0.15E-4	-0.27E-4	-0.19E-4	0.42E-4
18	3.6914	0.3747	-0.39E-8	-0.11E-6	-0.71E-6	-0.26E-5	-0.66E-5	-0.15E-4	-0.23E-4	-0.23E-5	0.81E-4
19	3.6869	0.4042	-0.41E-8	-0.13E-6	-0.83E-6	-0.30E-5	-0.74E-5	-0.16E-4	-0.18E-4	0.20E-4	0.14E-3
20	3.6800	0.4915	-0.65E-8	-0.20E-6	-0.13E-5	-0.44E-5	-0.11E-4	-0.18E-4	0.46E-5	0.10E-3	0.36E-3
21	3.6750	0.6207	-0.98E-8	-0.40E-6	-0.25E-5	-0.82E-5	-0.18E-4	-0.17E-4	0.64E-4	0.31E-3	0.84E-3
22	3.6700	0.7916	-0.22E-7	-0.10E-5	-0.60E-5	-0.18E-4	-0.31E-4	0.37E-4	0.31E-3	0.10E-2	0.19E-2
23	3.6650	0.9496	-0.52E-7	-0.24E-5	-0.14E-4	-0.37E-4	-0.28E-4	0.21E-3	0.93E-3	0.22E-2	0.34E-2
24	3.6550	1.1935	-0.24E-6	-0.93E-5	-0.43E-4	-0.62E-4	0.28E-3	0.14E-2	0.36E-2	0.53E-2	0.77E-2
25	3.6500	1.3335	-0.58E-6	-0.20E-4	-0.75E-4	0.14E-4	0.84E-3	0.31E-2	0.57E-2	0.81E-2	0.11E-1
26	3.6450	1.4252	-0.10E-5	-0.31E-4	-0.10E-3	0.18E-3	0.15E-2	0.48E-2	0.72E-2	0.11E-1	0.13E-1
27	3.6400	1.5126	-0.18E-5	-0.47E-4	-0.11E-3	0.54E-3	0.27E-2	0.68E-2	0.95E-2	0.14E-1	0.15E-1
28	3.6350	1.5835	-0.34E-5	-0.70E-4	-0.16E-4	0.13E-2	0.51E-2	0.90E-2	0.13E-1	0.16E-1	0.17E-1
29	3.6300	1.6545	-0.41E-5	-0.87E-4	-0.31E-5	0.15E-2	0.57E-2	0.97E-2	0.14E-1	0.17E-1	0.17E-1
30	3.6275	1.6789	-0.31E-5	-0.63E-4	0.36E-3	0.29E-2	0.90E-2	0.13E-1	0.18E-1	0.18E-1	0.15E-1
31	3.6217	1.7407	-0.48E-5	-0.92E-4	0.36E-3	0.29E-2	0.90E-2	0.13E-1	0.19E-1	0.21E-1	0.21E-1
32	3.6150	1.8503	-0.12E-4	-0.16E-3	0.81E-3	0.45E-2	0.11E-1	0.15E-1	0.20E-1	0.19E-1	0.18E-1
33	3.6101	1.9072	-0.15E-4	-0.95E-4	0.20E-2	0.73E-2	0.15E-1	0.19E-1	0.22E-1	0.20E-1	0.18E-1
34	3.6065	1.9400	-0.12E-4	0.34E-5	0.29E-2	0.97E-2	0.19E-1	0.25E-1	0.30E-1	0.27E-1	0.22E-1
35	3.6010	2.0037	-0.12E-4	0.18E-3	0.45E-2	0.13E-1	0.22E-1	0.30E-1	0.32E-1	0.28E-1	0.18E-1
36	3.5961	2.0656	-0.22E-4	0.47E-4	0.37E-2	0.12E-1	0.18E-1	0.27E-1	0.27E-1	0.22E-1	0.74E-2
37	3.5925	2.1176	-0.18E-4	0.84E-3	0.67E-2	0.17E-1	0.21E-1	0.26E-1	0.22E-1	0.17E-1	0.68E-2
38	3.5900	2.1346	-0.24E-4	0.35E-3	0.52E-2	0.15E-1	0.20E-1	0.29E-1	0.26E-1	0.18E-1	-0.21E-2
39	3.5813	2.2610	0.10E-3	0.42E-2	0.18E-1	0.40E-1	0.43E-1	0.51E-1	0.35E-1	0.78E-2	-0.19E-1
40	3.5534	2.5591	0.13E-2	0.31E-1	0.62E-1	0.78E-1	0.75E-1	0.25E-1	-0.22E-1	-0.23E-1	-0.11E-1

this is no doubt a fairly good treatment. This approximation turns out to have large deviation from the real situation only for the low excitation states of neutral helium. It is predictable that the quasi-hydrogen atom approximation only brings into the equation of state and the relevant thermodynamic quantities very limited affection, however, it has the very good advantage that, instead of interpolated with the pre-computed tables, the equation of state and the thermodynamic quantities can be calculated on the mesh in real time. The radiative opacity used in this work is a analytic formula to approach the OPAL tables (Rogers & Iglesias 1992) and the low temperatures opacity tables (Alexander et al. 1994). This analytic expression gives a smooth connection of OPAL table at intermediate and high temperature region and that of Alexander et al. (1994) in low temperatures region. The surface boundary for pulsation calculations are set at $\tau = 0.01$, and the bottom one is located at a temperature of $T \sim 5 \times 10^6 K$.

3.1 Pulsation stability

The distribution of the pulsationally stable and unstable models in HRD from our calculations is shown in fig. 1, where the tiny solid dots are stable models from the fundamental through the 4th overtone ($r_i < 0$, $i = 1, 4$); while the open circles, crosses, triangles, inverse triangles and squares are the unstable models respectively in the fundamental mode to the 4th overtone. Two separate instability strips can be seen clearly in the plot. The one of them in the middle of fig. 1 is the well known δ Scuti instability strip which is not really the topic of current work. As the δ Scuti strip is calculated using the same scheme, showing it here assures the reliability of our theory and the numerical scheme. The second one is the pulsating red giant instability strip on the upper-right of the figure. All the models between the two strips are all pulsationally stable at least for modes up to the 4th overtone. For RGB stars with low luminosity, the fundamental and the first overtone are both stable. These stars are unstable only in high order overtones. For high

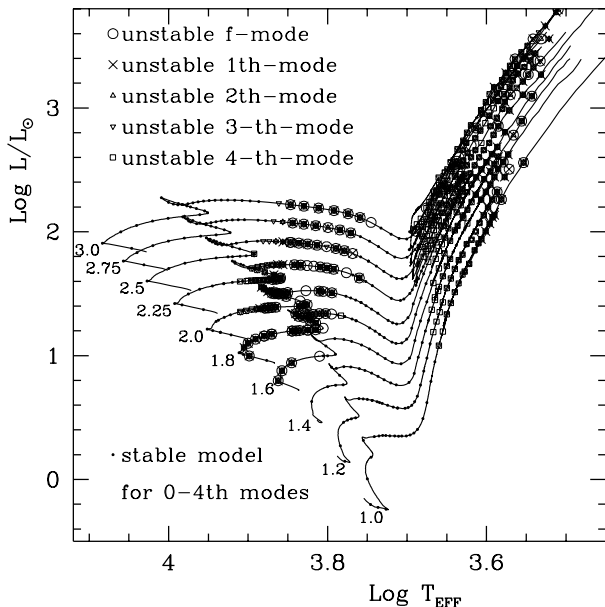


Figure 1. The distribution of pulsationally stable and unstable stars in the HRD. The tiny dots are pulsationally stable stars from the fundamental up to 4th overtone, the open symbols of circles, plus, triangles, inverse triangles and squares are respectively the unstable stars in the fundamental up to the 4th overtone.

luminosity and lower effective temperature stars (going up along the RGB and AGB), pulsation instability shifts towards lower overtone and the fundamental mode.

It follows from table 1 and fig. 1 that all the modes lower than the 5th order modes are stable for the $M = 1.0M_{\odot}$ RGB stars with $\log T_e \geq 3.66$. This agrees well with the observations of Henry et al. (2000). For stars with higher masses, the blue edge of the red giant instability strip shifts to higher temperature and higher luminosity. For a $M = 3M_{\odot}$ RGB star, the blue edge of instability strip moved to $\log T_e \approx 3.68$.

It has to be bared in mind that the location of the blue edge of the red giant instability strip depends not only on stellar mass, but also on metallicity. For increasing (decreasing) metallicity, the blue edge moves to red (blue). We did similar calculations for intermediate or low luminosity stars in globular clusters ($Z = 10^{-4}$) and we found that all RGB stars below the HB are stable in the fundamental mode while oscillating in 2-4th overtones, in that case the blue edge was shifted to $\log T_e = 3.74$ (Xiong & Deng 2006a,b). The 2 small amplitude short period red variables K1098 and VZ1140 found in M15 and M3 (Yao & Qin 1993, Yao, Zhang & Qin 1993) are both located near the intersection of HB and RGB, and their periods of the fundamental mode are both greater than 1 day according to theoretical calculations. However, the observed periods are respectively 0.5155 and 0.35 days, therefore suggesting that they are very likely pulsating at 2nd to 4th orders overtone. This agrees with the prediction of our work.

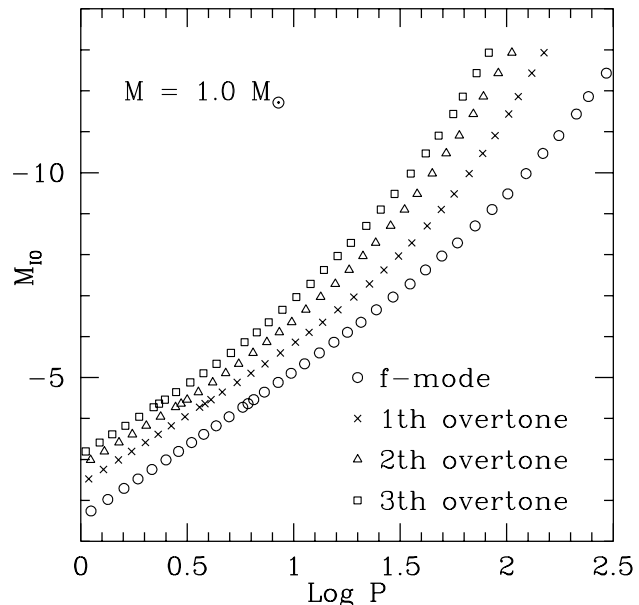


Figure 2. The period–luminosity relation for the evolutionary sequence of a $1M_{\odot}$ star. The horizontal axis is the logarithmic period, and the vertical one is the the reddening free Wesenheit index (Soszyński et al. 2004). The circles, plus signs, triangles and squares represent respectively the fundamental up to 3rd overtone.

3.2 Pulsation period and constant

The pulsation period can be derived from pulsation calculations. It is then straightforward to build a theoretical period-luminosity relation. However, to make such relation ready to be compared with that of observations is not so easy. In fig. 2, the theoretical period-luminosity relation for a $M = 1.0M_{\odot}$ RGB model is given. The horizontal axis is the pulsation period, and the vertical one is the reddening free Wesenheit index W_I (Soszyński et al 2004)

$$W_I = I - 1.55(V - I)$$

The temperature to color index conversion and the bolometric correction is taken from Johnson (1966). It can be found that the overall result of our calculations looks very similar to the observational one made for the red giant variables in Magellanic clouds (Soszyński et al. 2004). Unfortunately, quantitatively accurate comparison between our theoretical result and the observational relation is not possible for now due to the following reasons,

- (i) The temperature of the RGB stars depends critically on the metallicity, low temperature opacity and the mixing length parameter α . Larger metallicity and higher opacity, or smaller mixing length parameter α , will make the RGB move towards lower effective temperature;
- (ii) For low temperature RGB stars, both the effective temperature to color index conversion and bolometric correction are the worst determined, and this is especially true for AGB stars usually having a circumstellar dust envelopes which complicated the problem;
- (iii) The stars in the Magellanic clouds are not at all a group of stars having the same mass, age and chemical com-

position. Instead, they have all combinations of all those parameters.

In practice, the ratios between different overtones is a far better predictable than the periods, because they are less affected by stellar parameters. Figs. 3a and 3d are the theoretical Petersen diagrams from our calculations. A direct comparison shows that our results are very similar to the observations for the OSARG in LMC (Soszyński et al. 2004). Therefore we make a further speculation. There are the 4 ridges of period-luminosity relations in their fig. 7. We identify that the ridge (or sequence) a_1 (b_1) is the 1st overtone, a_2 (b_2) is the 2nd overtone, while a_3 (b_3) is a mixture of the 3rd and 4th overtones, and a_4 and b_4 are the 5th overtone. In fact, P4 in their paper should be the 5th instead of 4th overtone, because for the 4th overtone, it is not possible to have ratios of P4/P1, P4/P2 and P4/P3 being as small as 0.39, 0.56 and 0.76 respectively. However, if one considers that P3 in their paper is a mixture of 3rd and 4th overtones, while P4 is the 5th one, then a perfect match between the observations and our theoretical model.

Relative to pulsation period, the pulsation constant Q changes less, since it is only a slow varying function of stellar mass, luminosity and effective temperature. Fig. 4a shows the pulsation constants Q_i ($i=0-3$) of the fundamental mode through the 3rd overtone as functions of effective temperature, calculated for 4 sets of RGB models with masses of 1, 1.4, 2.0 and $3.0 M_\odot$ respectively, and with the same luminosity $L = 1000L_\odot$. From fig. 4a, the pulsation constants of 1st–3rd overtones changes relatively smaller than the fundamental mode does. The pulsation constants grow slowly with decrease of effective temperature for these overtones. While for the fundamental mode, on the contrary, The pulsation constants change largely with complex pattern, being a non-monotonic function of effective temperature, but showing a tendency of slight decrease with increase of mass.

Fig. 4b shows the pulsation constant as a function of luminosity for 4 sets of models of red giant models with the same temperature $\log T_e = 3.55$ but the different masses. Similarly, the pulsation constants of the 1st–3rd overtones are almost unchanged, while the fundamental mode shows a much larger variation, the pulsation constants increase with increase of luminosity of stars.

To further explore how the pulsation constant changes with stellar parameters such as mass, luminosity and effective temperature, 24 sets of models of red giant are calculated as a supplementary database for this aim. They consist of 600 models with different masses ($M = 1, 1.4, 2.0$ and $3.0 M_\odot$), luminosities ($\log L/L_\odot = 2.6-3.5$) and effective temperature ($\log T_e = 3.40-3.70$). we get the following analytic fitting formula for pulsation constant,

$$\begin{aligned} \log Q = & \sum_{n=0}^3 a_n t^n + m \sum_{n=0}^3 b_n t^n \\ & + \left[\sum_{n=0}^3 c_n t^n + m \sum_{n=0}^3 d_n t^n \right] l \\ & + \left[\sum_{n=0}^3 e_n t^n + m \sum_{n=0}^3 f_n t^n \right] l^2, \end{aligned} \quad (21)$$

where

Table 2. coefficients in Eq.(21)

F	mode	1th	2th	3th
a0	-1.193	-1.451	-1.625	-1.728
a1	+0.80	-0.69	-0.80	-0.60
a2	+2.0	+0.34	+0.20	-0.18
a3	-45	+17	+20	+7.0
b0	-0.19	-0.075	+0.05	0.0
b1	-2.90	+0.96	+0.55	+0.65
b2	-2.75	+0.28	-5.0	-4.0
b3	+110	-28	0.0	0.0
c0	+0.34	-0.015	-0.04	+0.01
c1	+0.70	-0.10	-0.17	-0.49
c2	-10	+1.3	+3.0	+1.7
c3	-50	0.0	0.0	+10
d0	-0.80	+0.15	+0.06	-0.08
d1	0.00	+0.30	+0.75	-0.89
d2	+45	+4.0	-4.4	-3.2
d3	+50	0.0	0.0	+90
e0	+0.18	-0.06	+0.04	+0.06
e1	-3.5	0.0	+0.27	0.0
e2	-21	0.0	0.0	0.0
e3	+190	0.0	0.0	0.0
f0	-0.36	+0.05	-0.37	-0.32
f1	+12	-1.0	-1.7	-1.3
f2	+59	0.0	+16	+22
f3	-650	0.0	0.0	-650

$$m = \log M/M_\odot,$$

$$t = \log T_e - 3.55,$$

$$l = \log L/L_\odot - 3.0.$$

The coefficients in above expressions, $(a-f)_n$, from the fundamental to the 3rd overtone are given in table 2. Figs. 5a and 5b demonstrates the difference $\Delta \log Q_i = \log Q_i - \log Q_{i,ap}$ ($i=0-3$) between the calculated pulsation constants Q_i for the nearly 600 models and their analytic fitting $Q_{i,ap}$ as functions of effective temperature $\log T_e$ (5a) and luminosity (5b). It is clear from fig. 5 that a pretty good fitting is secured in the domain defined by $1 \leq M/M_\odot \leq 3$, $3.4 < \log T_e < 3.7$ and $2.6 < \log L/L_\odot < 3.5$.

4 THE EXCITATION MECHANISM FOR THE RED GIANT VARIABLES

By using a work diagram, the excitation and damping on the oscillations of stars due to different factors can be clearly illustrated and analysed quantitatively. The definition and derivation of the integrated work (IW) can be found in the Appendix. The total IW W_{all} is composed of the following 3 components,

$$W_{all} = W_P + W_{Pt} + W_{vis} \quad (22)$$

where W_P is the pressure component (including radiative pressure), W_{Pt} is the turbulent pressure one, while W_{vis} is that of turbulent viscosity, all being functions of depth (M_r or $\log P$). In our work, the IW is counted from the stellar center and integrated outwards, therefore the total IW W_{all} at the surface should be the growth rate of pulsation amplitude $\eta = -2\pi\omega_i/\omega_r$, where ω_i and ω_r are respectively

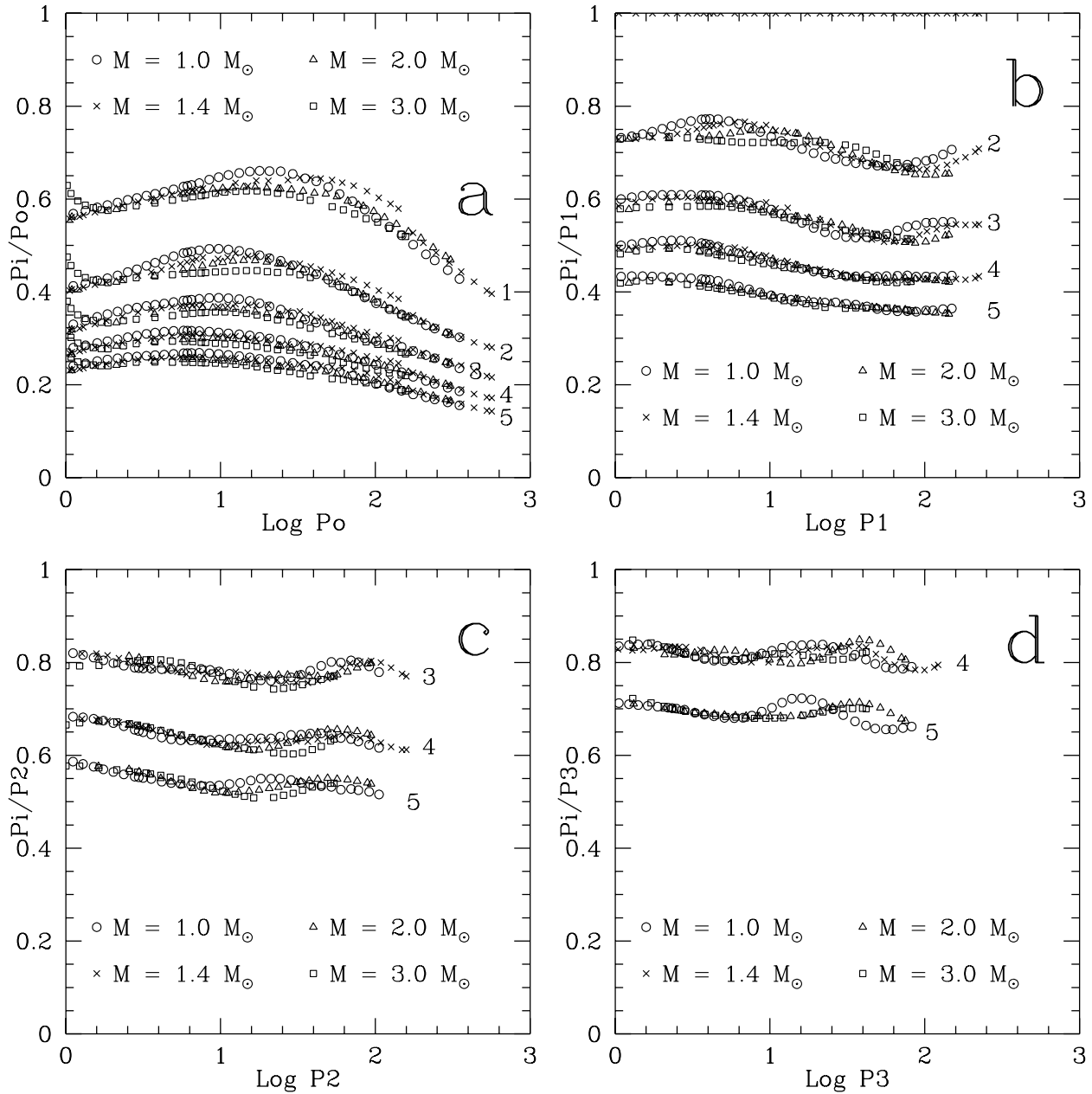


Figure 3. The theoretical Peterson diagram for evolutionary model sequence. Plotted are the period ratios P_j/P_i ($i = 0, 1, 2, 3$; $j = i - 1, \dots, 5$) versus $\log P_i$. The 4 panels have different i indices, a) $i = 0$ the fundamental mode; b) $i = 1$ the 1st overtone; c) $i = 2$ the 2nd overtone; and d) $i = 3$ the 3rd overtone. The circles, plus signs, triangles and squares are respectively the sequences for $M=1, 1.4, 2.0$ and $3.0M_\odot$.

the real imaginary and real part of the complex pulsation frequency $\omega = i\omega_i + \omega_r$, i.e.,

$$\eta = W_{all}(M_0) \quad (23)$$

When $W_{all}(M_r)$ (or its one component) increases outwards, this region is therefore a pulsational excitation zone (of the corresponding component), otherwise it will be a damping zone.

It is well known that the quasi-Cepheid variables (including Cepheids of populations I and II, RR Lyrae and δ Scuti stars. this term will be used hereafter) are excited by the κ mechanism. The existence of the blue edge of the

instability strip is due to the fact, when stellar surface temperature is too high, the ionization zones of hydrogen and helium that is responsible for κ mechanism are very near the surface, their mass and heat capacity are too small, and they produce far less excitation that is not enough to compensate the damping at the deep interior, therefore oscillations cannot excited for these hot stars. This is shown by the plot of IW versus depth in fig. 6 for a hot star ($M = 2.0M_\odot$, $\log L/L_\odot$ and $\log T_e = 3.9222$) located outside the blue edge of the δ Scuti instability strip. It can be seen from fig. 6 that convection in the whole envelope is negligible. In the deep interiors below the second ionization zone of helium,

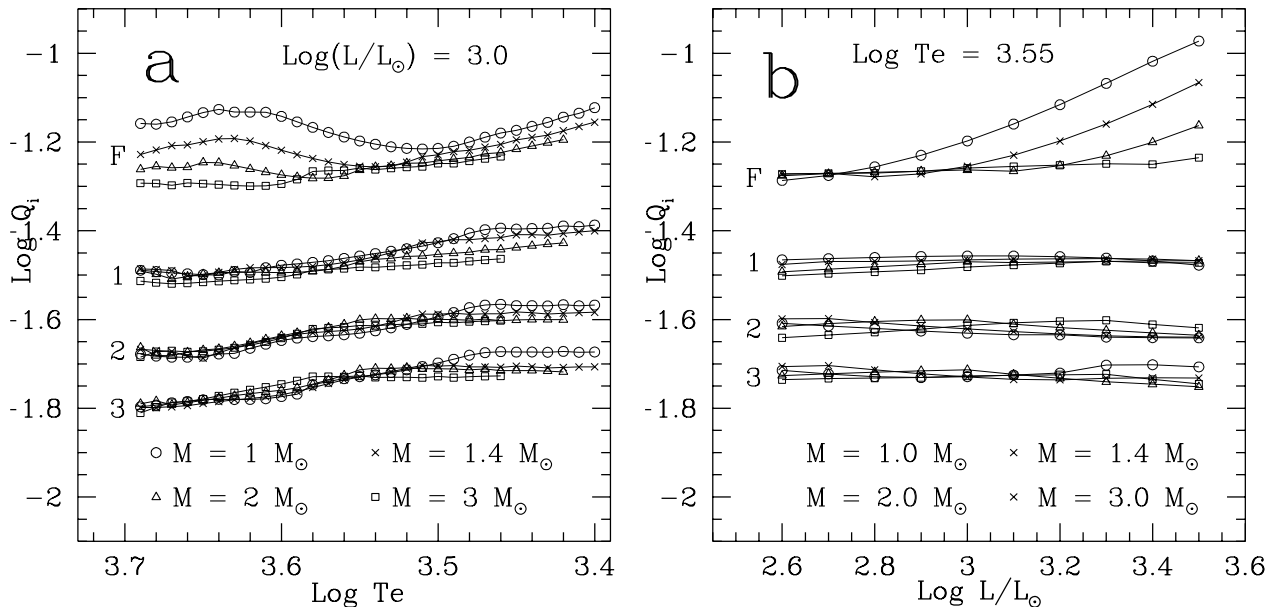


Figure 4. a) The pulsation constants from the fundamental model to the 3rd overtone mode as functions of effective temperature at a given luminosity of $\log L/L_{\odot} = 3.0$. b) The pulsation constants as functions of effective luminosity at a given effective temperature of $\log T_{\text{eff}} = 3.55$. The circles, plus signs, triangles and squares are respectively for $M=1, 1.4, 2.0$ and $3.0M_{\odot}$.

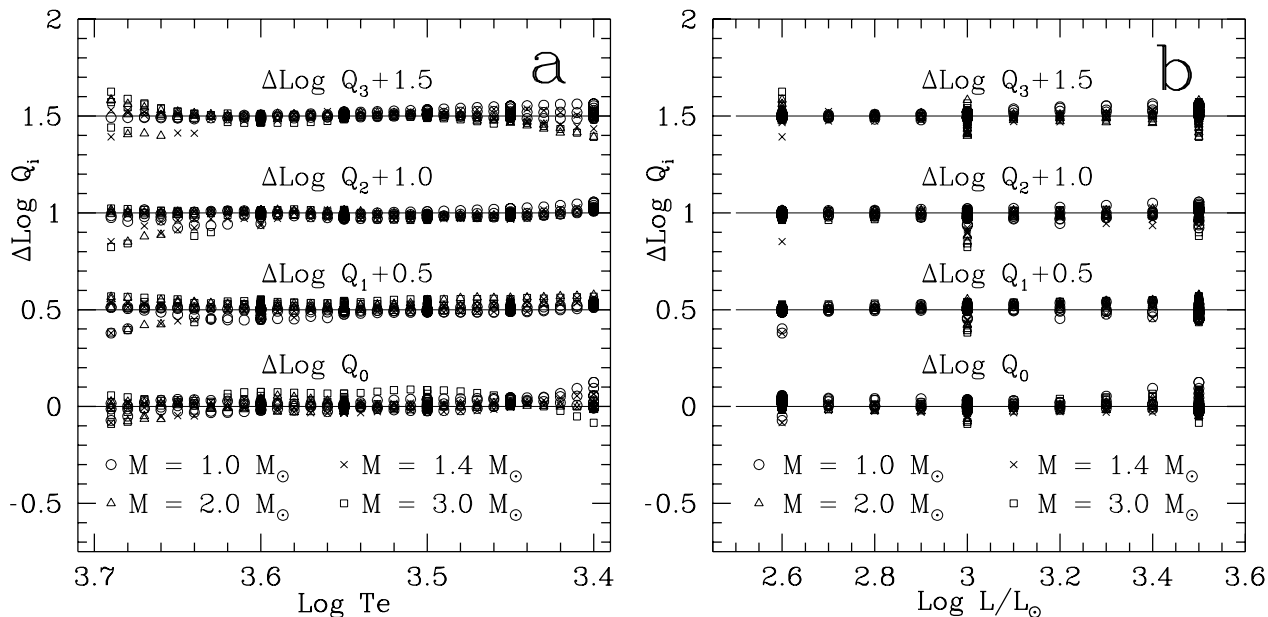


Figure 5. The deviations of the analytic fitting (eq. [21] in the text) of the pulsation constants from the values given by calculations of oscillations, $\log Q_i = \log Q_i - \log Q_{i,ap}$, ($i=0-3$), a) as a function of effective temperature; and b) as a function of luminosity. solid dots for $M=1M_{\odot}$, plus signs $1.4M_{\odot}$, triangles $2.0M_{\odot}$ and squares $3.0M_{\odot}$.

the overall trend of the integrated work W_P is decreasing towards the surface of star due to the radiation damping. Near $\log P = 8$, the W_P curve shows an abrupt ascending followed by a quick descending, this is due to the iron absorption peak over there. For $\log P \sim 6.0-4.0$, W_P increases quickly, and it is excited by the κ mechanism in the first and second ionization zones of helium. There is a little rise up at $\log P \sim 4.0$ which is made by the κ mechanism due to

ionization of hydrogen. Nevertheless, all the excitation in the ionization zones of hydrogen and helium are not enough to compensate the radiation damping arise from the deep interiors, this makes $W_P < 0$ for this model, therefore the star is pulsationally stable.

The ionization zones of hydrogen and helium go deeper inside with decrease of effective temperatures of stars, their total mass and heat capacity become larger, therefore ex-

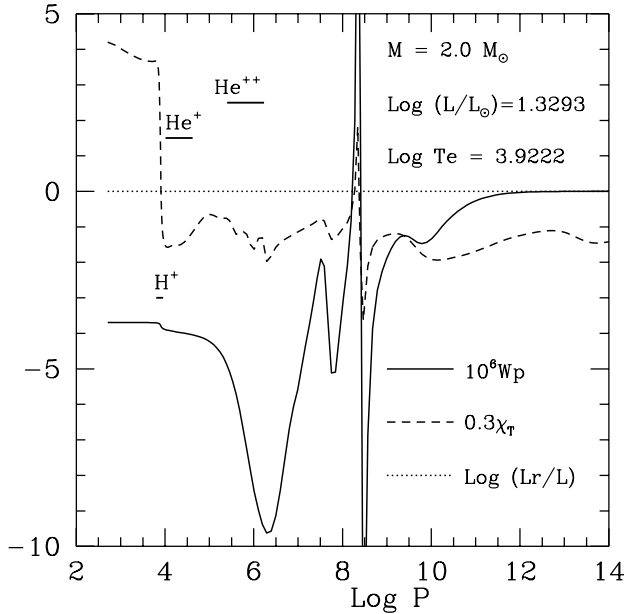


Figure 6. The integrated work (IW) of the fundamental mode for a hot star located outside the blue boundary of the δ Scuti instability strip. The solid line is the integrated work (IW), dashed line the opacity, and dotted line the fractional radiation flux L_r/L as functions of depth ($\log P$). The 3 heavy horizontal line on the upper left part of the figure represent the locations of the ionization zones of hydrogen and the two of helium.

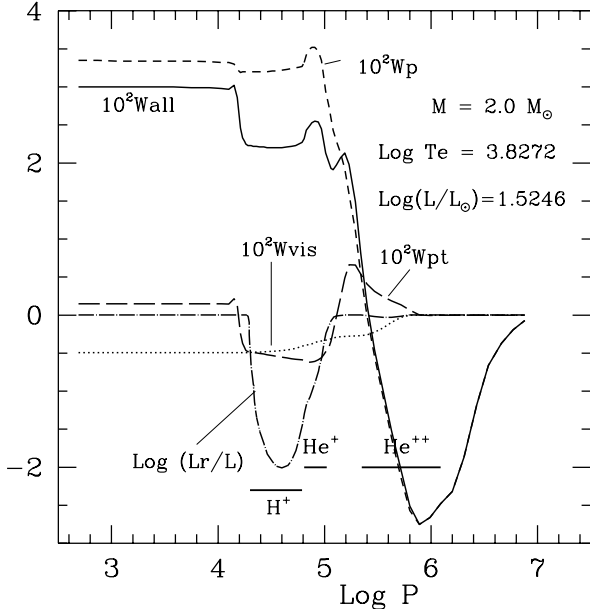


Figure 7. The integrated work (IW) of the fundamental mode for a warm star within the δ Scuti instability strip as a function of depth (the solid line). The runs of W_P (the dashed line, gas pressure component), W_{Pt} (the long dashed line, turbulent pressure component), W_{vis} (dotted line, turbulent viscosity component), and $\log L_r/L$ (dot-dashed line) are also shown. The parameters including mass, luminosity and effective temperature of the star are labeled. The coupling between convection and oscillations has been taken into account.

citation gets enhanced. When the excitation takes over the radiation damping in the deep interior, stars will become pulsationally unstable. Fig. 7 depicts IW versus depth for a warm star within the δ Scuti instability strip ($M = 2.0M_\odot$, $\log L/L_\odot = 1.5246$ and $\log T_e = 3.8272$). This star possesses a relative shallow convective zones of the hydrogen and first helium ionization. The second ionization zone of helium is radiative in this case. Around $\log P = 5.5$ both W_P and W_{all} increase quickly outwards due to the exciting of the second ionization zone of helium. The convection component (W_{Pt} and W_{vis}) is much smaller than the excitation due to radiation. This excitation is also greater than the radiation damping in the deep interiors, therefore the star become unstable.

Going to even lower effective temperatures, convection zone in stars becomes deeper. When the second ionization zone of helium becomes complete convective, the excitation due to radiation κ -mechanism reduced largely. In the deep interior, however, the thermodynamic coupling between convection and oscillations works now as a damping for pulsation that makes the star stable, this is true at least for the fundamental and the first overtone. The IW for a yellow giant ($M = 2.0M_\odot$, $\log L/L_\odot = 1.3426$ and $\log T_e = 3.7368$), which locates in between the δ Scuti and the pulsating red giant instability trips, is shown in fig. 8. Our calculations demonstrate that this star is stable at least in the first 7 low order overtones.

With even lower effective temperature and higher luminosity, pulsation instability moves to lower order modes. In figs. 9a–9d shows IW of the fundamental and the first 3 overtone modes versus depth for a star on the RGB ($M = 2.0M_\odot$, $\log L/L_\odot = 2.3451$ and $\log T_e = 3.6301$). For red giant stars, the pulsation amplitude decreases very quickly going downwards from the surface, and tends to vanish at the center. The effective pulsation region can be seen directly from the IW plot, in which the radiative flux is much smaller than the convective one. This infers that the gas pressure component of IW, W_P , mainly comes from the thermodynamic coupling between convection and oscillations. In the deep interior ($\log P \geq 5$), the general trend of W_P is to decrease with decreasing $\log P$, meaning that the thermodynamic coupling between convection and oscillations functions as a damping. Near to the stellar surface, W_P increases outwards, that is resulted from the radiative modulation excitation in the radiative flux gradient zone (Xiong, Cheng & Deng 1998). It is clear from figs. 9a–9b that, for these red giant stars, the effects of radiation and the thermodynamic coupling between convection and oscillations (W_P) are already much smaller than that of dynamical coupling (W_{Pt} and W_{vis}). For red giants with intermediate to low luminosity, $W_{Pt} (>0)$ and $W_{vis} (<0)$ have similar absolute value while having opposite signs. The fundamental and the first 2 overtone modes have $W_{all} < 0$, therefore are pulsationally stable; for modes higher than the 3rd overtone, however, $W_{all} > 0$ therefore the stars become unstable. As shown in table 1, all the low order modes are stable for low luminosity red giants which are unstable only at the high order overtones. Going to stars of higher luminosity and lower effective temperature, pulsation instability shifts steadily towards lower order modes, the pulsational amplitude growth rates increase very quickly. For the luminous Mira variables the fundamental mode and the low

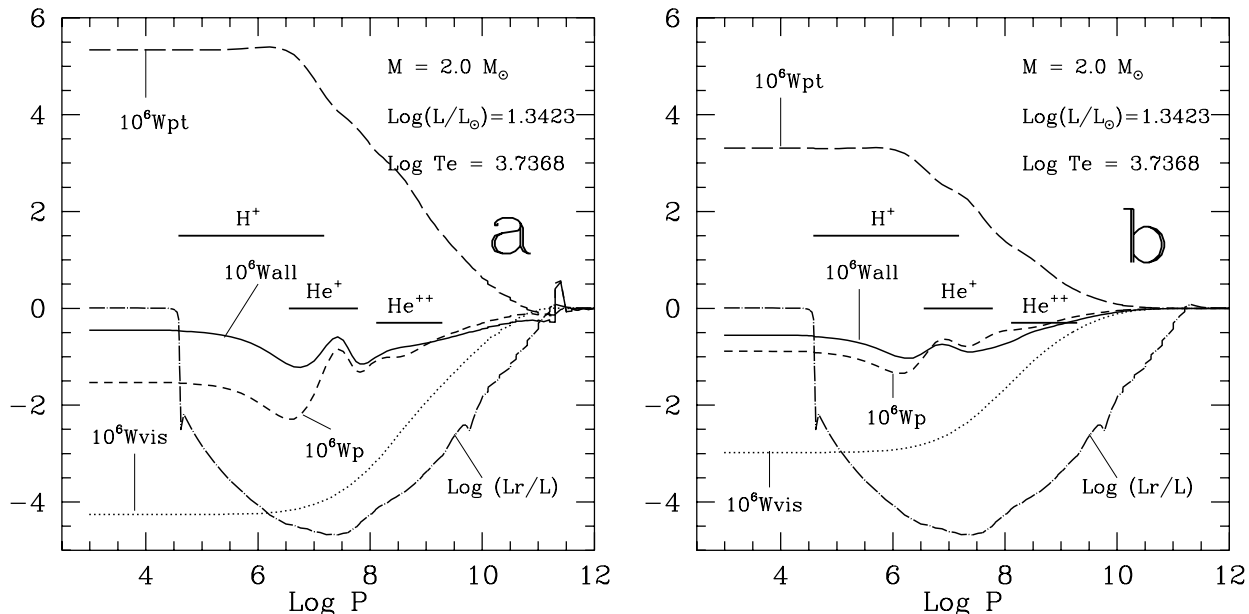


Figure 8. Similar to fig. 7, but for the integrated work (IW) as a function of depth for a pulsationally stable star located in between the δ Scuti instability strip and the PRG instability strip. a) the fundamental mode; b) the 1st overtone.

oder overtones are only linear unstable modes, all the modes above 4th order become stable (Xiong, Deng & Cheng 1998). Such a trend is marginally shown in fig. 1 because only the first 5 pulsation modes are displayed, and no pulsation stability coefficients can be given. Table 1 is can make up this shortcoming, which shows that all modes below 8th overtone are pulsationally stable for all population I stars with $M = 1.0M_{\odot}$ and $\log T \geq 3.70$. It is clearly shown from table 1 that the pulsation instability shifts towards lower order modes and amplitude growth rates increase with increase of luminosity and decrease of effective temperature of stars. Due to numerical difficulties, we unfortunately could not construct equilibrium model for high luminosity red giants under complete non-local treatment of convection. The most luminous and coolest model got by us is No.40 in the table. However, the general trend mentioned above can be seen confidently from the table 1 and fig. 1. This trend agrees well with our previous work on the luminous long period variables (Xiong, Deng & Cheng 1998). The only difference between previous and the current works is the constructing of the equilibrium model, the non-adiabatic oscillations are calculated in exactly the same way: both are treated with our non-local convection theory. As discussed in the previous section, the amplitude growth rates of SARVs are smaller than those of luminous Miras by 1–3 orders of magnitude, very special care is required in the current work where all the static equilibrium models for the non-adiabatic oscillations of SARVs are computed using our complete non-local convection theory. However, the approximate quasi non-local convection models are applied in the previous work for the high luminosity LP variables, which is a modification of the local convection models. In the convectively unstable zone, all the convective quantities in the quasi non-local models take the same value as in the local convection models, while in the overshooting zone, they are extended from the lo-

cal models following a analytic asymptote of the properties of overshooting outside the unstable zone. Comparing the numerical calculations between local and non-local models, it shows that within a convectively unstable zone, they are rather close to each other, with the sensible difference only near the boundaries and in the adjacent overshooting zones (Xiong 1989b). For luminous red variables having very large pulsation amplitude growth rates, such a approximate treatment may induce a certain amount of uncertainty to value of the growth rates, however, the qualitative results on the stability of these stars will not be affected. The numarical tests confirm this inference.

By the way, the so-called frozen convection approximation is still favored by some workers (Gong et al. 1995) in the study of non-adiabatic oscillations of stars. They assume that convection is unchanged during the course of stellar oscillations. Such an approximation is correct only when the pulsation timescale is much smaller than that of convective motion. Unfortunately, these timescales are usually the same order of magnitude within the convective zones. Therefore it is clear that this kind of treatment must be incorrect in most cases, especially for analyzing the instability of the low temperature stars with extended convective envelopes. The only chance for the frozen convection approximation to be reasonable is for the study of the blue edge of the instability strip, because for hot star near the blue edge, convection zone is rather shallow so that radiation dominates, and the coupling between convection and oscillations has little influence on the stability of these objects. In any case, this approximation can explain neither the red edge of the Cepheid instability strip, nor the blue edge of the pulsating red giant instability strip. We would like to conclude confidently that if the coupling between convection and oscillations is excluded, namely the frozen convection approximation is applied, all stars located to the red side of the blue edge of the

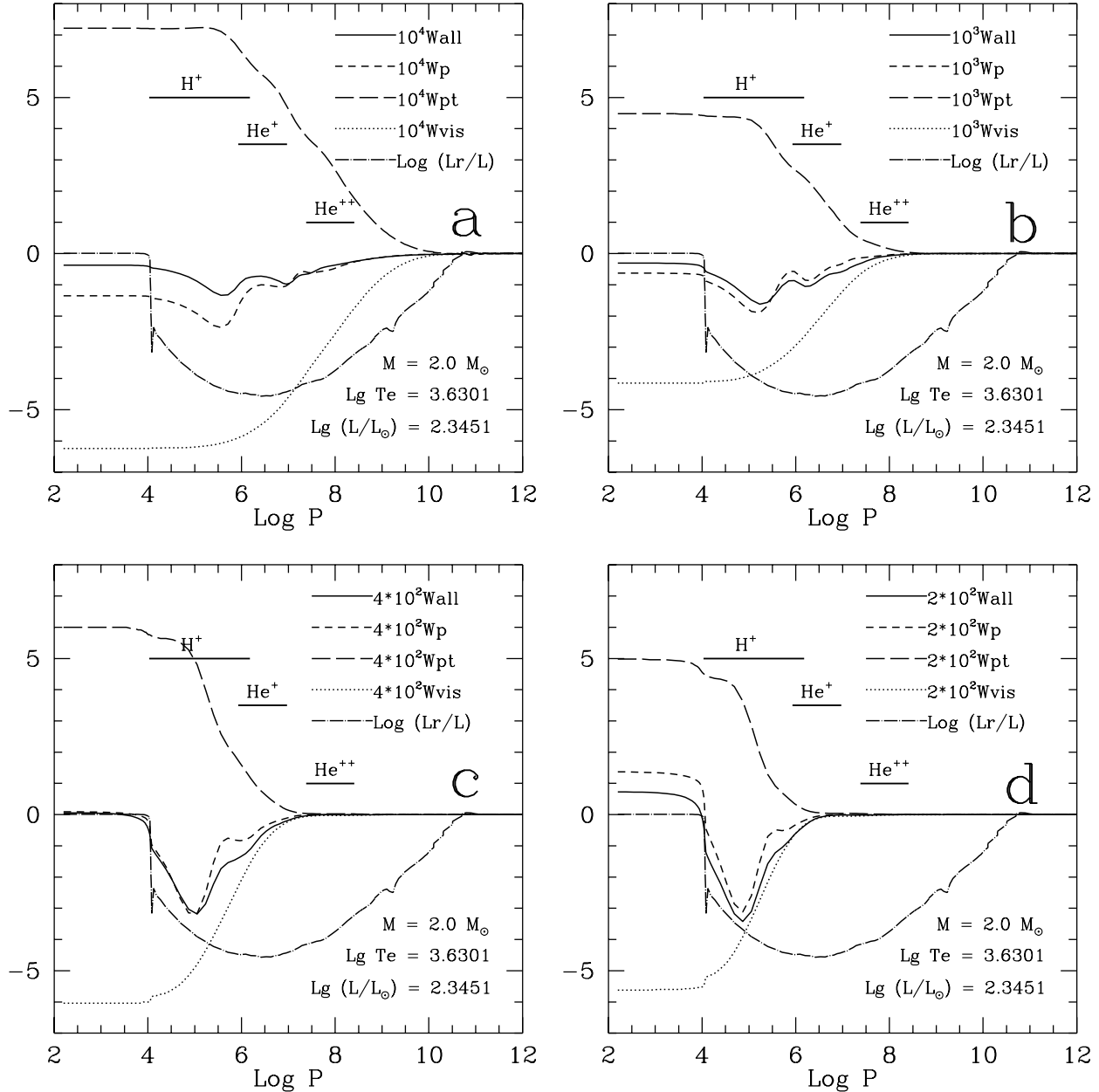


Figure 9. Similar to fig. 7, but for a RGB star. a) the fundamental mode; b) the 1st overtone; c). the 2nd overtone; d) the 3rd overtone.

Cepheid instability strip in the HRD will be pulsationally unstable.

Figs. 10a and 10b display the IW versus depth for the fundamental and the 1st overtone of the same stable star as in fig. 8, which is located in between the δ Scuti and the red giant instability strips, but the coupling between convection and oscillations is not considered in this calculation. In fig. 10a, there are two rapid increase of IW in the surface and bottom boundaries of the convection zone. They are resulted from the radiative modulation excitations produced in the radiative flux gradient regions. Although being a result of radiative flux and related to opacity, the radiative modulation excitation is completely distinct from the radiative κ mechanism. The former one exists only in the radiative flux gradient region whose functionality can be found in our

previous work (Xiong, Cheng & Deng 1998). Obviously, the ionization zones of hydrogen and helium where κ mechanism operates, are now fully convective, in that the radiative flux is only a tiny fraction of the total flux. As shown in fig. 10a, W_P is virtually a horizontal line in the ionization zones of hydrogen and helium. In the deeper interior, radiation ought to be a damping, but in the radiative flux gradient region just inside the lower boundary of the convective zone, W_P shows a abrupt jump. This is a good evidence to show that the radiative modulation excitation is not the usual κ mechanism. For the 1st overtone (fig. 10b), W_P shows only a single abrupt jump inside the upper boundary of the convective zone. This is due to the fact that oscillations tend to be in further outer layer for the 1st overtone than the fundamental mode, near the lower boundary of convective zone,

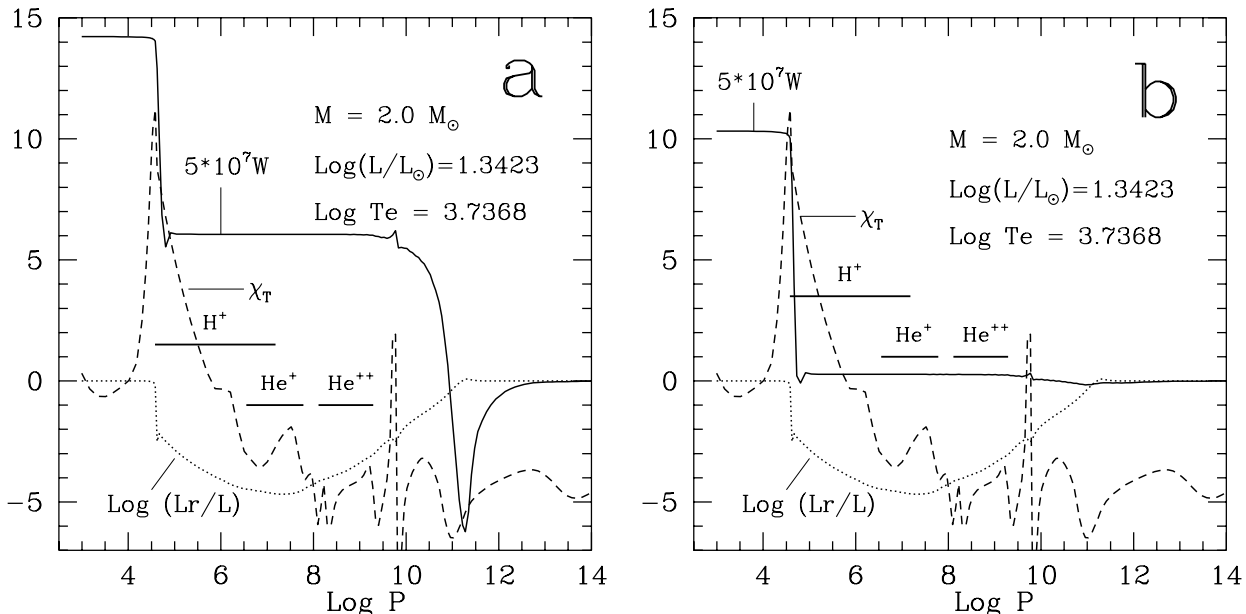


Figure 10. The integrated work (IW) as a function of depth for the same star as fig. 8, but without taking into account the coupling between convection and oscillations. a) the fundamental mode; b) the 1st overtone.

the pulsation amplitude is already very small, the radiative modulation excitation is therefore much less.

Figs 8a and 8b show the IW versus depth for the same stellar model as the one described in above paragraph, but having the coupling between convection and oscillations taken into account. There is no any similarity in the shapes of IW shown in fig. 8 and fig. 10. In fig. 8, the absolute values of W_{Pt} and W_{vis} are both much greater than that of W_P , and the W_P curve runs completely in a different form from that in fig. 10. This difference is caused by coupling between convection and oscillations. The effects of radiation have already overwhelmed by that of convection for these low temperature stars.

5 CONCLUSIONS AND DISCUSSION

In this work, we have studied the linear non-adiabatic oscillations of the evolutionary models with $M = 1 - 3M_{\odot}$ using a non-local time-dependent theory of convection. The excitation mechanism for the instabilities are studied. The main results can be concluded in the following,

(i) Two separate pulsational instability strips are found in the HRD: the hotter one is the δ Scuti instability strip, while the cooler one is the pulsating red giant instability strip. The two strips are intercepted by a region of pulsationally stable (at least from the fundamental up to the 4th overtone) yellow giants;

(ii) The δ Scuti stars and the pulsating red giants (PRGs) are two distinct types of variables. The former one is excited by the radiative κ mechanism and the later one is driven by the coupling between convection and oscillations;

(iii) For the low luminosity PRGs, pulsations are in the high order modes. Going to lower effective temperature and

higher luminosity, pulsationally unstable modes shift gradually to lower orders from higher orders;

(iv) In the deep interior of convective zone far away from the boundary, generally speaking, the thermodynamic coupling between convection and oscillations is a damping against pulsation. This is the true reason for the existence of the red edge of the Cepheid instability strip. Roughly speaking, when convection zone extend below the second ionization zone of helium, the red edge of Cepheid instability strip shows up;

(v) Obviously, turbulent viscosity is always a damping against oscillations, whereas turbulent pressure is an excitation mechanism. The dynamical coupling between convection and oscillations plays a key role in exciting the oscillations of PRGs;

(vi) For the instability of the low temperature stars having extended convective zone, the coupling between convection and oscillations is absolutely a dominant factor. When the coupling is excluded, neither the red edge of the Cepheid instability strip nor the blue edges of the PRGs instability strip can be explained, and all stars on the right side of the red side of the blue edge of the Cepheid instability strip will be pulsationally unstable;

(vii) The theoretical Peterson diagram given in this work is very similar to that of observations by Soszyński et al. (2004). However, based on our calculations of period ratios, we would like to guess that very likely the P4 in their work is in fact the 5th overtone, while P3 is a combination of the 3rd and 4th overtones. For the observed modes with period ratio close to 1, no explanation can be made at this point.

PRVs are a group of low temperature red giant stars located outside the Cepheid instability strip in the HRD. Their exciting mechanism was not known in the past. Based on a non-local time-dependent theory of convection, the present work provides a natural solution that explains 2

types of variables of distinct properties: δ Scuti stars (and all the Cepheid like variables) and the PRGs. In previous section, we have addressed the existence of the red edge of the Cepheid instability strip, and the presence of another PRV instability strip at a lower temperature region in the HRD outside the Cepheids instability strip.

In the *General Catalogue of Variable Stars* (Kholopov et al. 1985–1990), the long period variables (LPVs) are classified as 3 primary types: Miras, semi-regulars (SRs) and irregulars (L). Following the statistical study of PRVs in the Galactic field and stellar group (stellar clusters and associations), Eggen (1973a,b, 1975, 1977) made another classification according to pulsation amplitude, which is again in 3 major types: Large-amplitude red variables (LARVs: $\Delta V > 2\text{mag.}$), medium-amplitude red variables (MARVs: $0.3 < \Delta V < 2\text{mag.}$) and small amplitude red variables (SARV: $\Delta V \leq 0.5\text{mag.}$), where the ones with visual amplitude less than 0.2 mag. and very short period (20–40days) may form a individual group. Based on the MACHO database, Wood (2000) discovered that the PRGs in LMC displayed 5 ridges (or sequences) of A, B, C, D and E in the $K - \log P$ diagram. The Miras, located in sequence C, have the largest amplitude and for sure represent the fundamental mode. Stars falling into sequence B are SRs possessing smaller amplitudes. In sequence C, one finds the stars with relatively smaller amplitudes ($\Delta V < 1.5\text{mag.}$), also being SRs. Stars with very small amplitudes ($\Delta V < 0.2$) falling in sequence A are very likely the SARVs as classified by Eggen. Sequences B and A may correspond to the 1st–3rd overtones (Wood, 2000). Soszyński et al. (2004, 2005) confirmed the discovery of Wood using OGLE-II and OGLE-III data, and they further pointed out that the OSARGs (OGLE small amplitude red giants=SARVs) and the LPVs (Miras) are two different types of pulsating stars. On the Period-Luminosity (PL) diagram (periods– W_I), the primary periods of OSARGs fall in sequences A and B, and none of the second and the third dominant period– W_I relation of OSARGs fall in sequences C; On the contrary, the primary period– W_I relation fall in sequences C and B, and none of the second and the third dominant period– W_I relation goes in sequence A. Based on classification as such, in the PL diagram of Wood’s ridges A and B of OSARGs, can be divided into 4 separate ridges a_1 , a_2 , a_3 and a_4 for OSARGs brighter than the tip of RGB, and b_1 , b_2 , b_3 and b_4 for OSARGs fainter than the tip of RGB. According to the theoretical Peterson diagram, it is confident to believe that ridge C is the fundamental model, a_1 (b_1) and a_2 (b_2) are respectively the 1st and the 2nd overtones. Whereas, a_3 and a_4 are not likely to be single mode sequence: a_3 (b_3) is a mixture of the 3rd and the 4th overtones, and a_4 (b_4) is a mixture of the 4th and the 5th overtones. Otherwise, as discussed in section 3, it is difficult to understand the observational Peterson diagram (Soszyński et al. 2004). As shown in fig. 3, the period ratios are hard affected by stellar mass, following similar arguments, they are neither affected by metallicity. Because metallicity determines only the location of the instability strip and the ML relation. As both mass and metallicity hardly influence the period ratios, our results for mode identifications should be reliable.

Observational evidence provided by Wood and Soszyński et al. demonstrate that there is a tight link between the properties of PRGs and their oscillation modes. It

is clear that primary period of Miras are in the fundamental mode (Soszyński et al. 2004), the primary period of SRs are either in the first overtone or the fundamental mode, the second the third dominant periods of them should not be higher than the 4th overtone. On the contrary, most of the of the SARGs are pulsating in the 3rd–4th overtones ($\sim 50\%$) or in the 2nd overtone ($\sim 20\%$), and their fundamental mode is pulsationally stable. How to inspect theoretically such observations?

Based on the theory of oscillations, when neglecting both rotation and magnetic field, the pulsation properties of stars depend primarily on luminosity and effective temperature, and secondarily on mass and metallicity. It follows from table 1 that, for the faint RGs, pulsation instability starts in high order overtones, and it shifts to lower orders with increase of luminosity and decrease of effective temperature, while the pulsation amplitudes also grows. By comparing the pulsational instability for different stellar masses, as shown in fig. 1, going towards higher masses, the blue edge of the instability shifts to higher luminosity and higher temperature. This theoretical results agree well the observations. Eggen (1977) studied the distribution in $M_{bol}-(R-I)$ diagram for PRVs in the Galactic field and stellar groups, and found out that the SARVs are indeed located in the high temperature ($0.8 \leq (R - I)_0 \leq 1.6$) and low luminosity region, the LARVs stay in the low temperature and high luminosity area, whereas MARVs stay in the intermediate region. Henry et al. (2000) also shown that all the K5–M0 giants are SARGs, they are located in the high temperature and low luminosity region in the HRD. Percy & Parkes (1998) studied the pulsation modes for 13 SARGs with well-determined period and accurate Hipparcos parallaxes, and claimed that 9 of the stars are pulsating in the 1st or the 2nd overtone, 1 in the 3rd overtone, while only 3 in the fundamental or the 1st overtone. Soszyński et al.’s observational study shown that non of all their OSARGs is oscillating in the fundamental mode. Therefore, it can be conclude that our theoretical predictions agree pretty well the observational trend. However, it is difficult to understand that, on the $\log P-M_I$ diagram of Soszyński et al. (2004), the OSARGs extends almost all the way to the brightest end. We have not yet understand OSARGs. Why they are so different from the Mira and SR variables at the same luminosity? It can be seen from fig. 1 that the blue edge of PRGs instability strip move toward higher temperature and luminosity with increase of stellar mass. OSARGs, we suppose, are more massive and hotter than Mira and SR variables with the same luminosity. The brightest OSARGs may be a group of younger massive red giants. If this guess is true, there should not be luminous OSARGs in the old clusters.

ACKNOWLEDGEMENTS

The Chinese National Natural Science Foundation (CNNSF) is acknowledged for support through grants 10573022, 10173013, 10273021 and 10333060.

REFERENCES

Alcock, C., et al., 2000, ApJ, 541, 734

Alexander, D.R. & Ferguson, J.W., 1994, ApJ, 437, 879
 Afonso, C., et al., 1999, A&A, 344, L63
 Balmforth, N.J., 1992, MNRAS, 255, 603
 Bond, I.A. et al, 2001, MNRAS, 327, 868
 Bressan, A., Fagotto, F., Bertelli, G. & Chiosi, C., 1993, A&AS, 100, 647
 Coini, M.-R.L., Marquette, J.-B. & Loup, C., 2001, A&A, 377, 945
 Cox, A.N. & Ostlie, D.R., 1991, Ap&SS, 210, 311
 Deng, L. & Xiong, D.R., 2006, ApJ, 643, 426
 Edmonds, P.D. & Gilliland, R.L., 1996, ApJ, 464, L157
 Eggen, O.J., 1969, ApJ, 158, 225
 Eggen, O.J., 1972a, ApJ, 174, 45
 Eggen, O.J., 1972b, ApJ, 177, 489
 Eggen, O.J., 1973a, ApJ, 180, 857
 Eggen, O.J., 1973b, ApJ, 184, 793
 Eggen, O.J., 1975, ApJ, 195, 661
 Eggen, O.J., 1977, ApJ, 213, 767
 Fox, M.W. & Wood, P.R., 1982, ApJ, 259, 198
 Gong, Z.G., Li, Y. & Huang, R.Q., 1995, AcASn, 15, 56
 Gough, D.A., 1977, ApJ, 214, 196
 Henry, G.W., Fekel, F.C. & Henry, S.M., 2000, ApJs, 130, 201
 Hinze, J.O., 1975, Turbulence (McGraw-Hill, New York)
 Johnson, H.L., 1966, ARA&A, 4, 193
 Jorissen, A., Mowlavi, N., Sterken, C. & Manfroid, J., 1977, A&A, 324, 578
 , Kholopov, P.N., et al., 1985–1990, General Catalogue of Variable Stars, 4th ed. (Moscow State University)
 Kiss, L.L. & Bedding, T.R., 2003, MNRAS, 343, L79
 Kiss, L.L. & Bedding, T.R., 2004, MNRAS, 347, L83
 Noda, S. & takeuti, M., Abe, F. et al., 2002, MNRAS, 330, 137
 Ostlie, D.A. & Cox, A.N., 1986, ApJ, 311, 864
 Percy, J.R. & Parkes, M., 1998, PASP, 110, 1431
 Percy, J.R., Nyssa, Z. & Henry, G.W., IBVS, 2001, No. 5209
 Percy, J.R. & Bakos, A.G., 2003, in Garrison Festschrift Conf. eds. R.O. Gray, C.J. Corbally & A.G.D. Philip (Davis press), p.49
 Pojmanski, G., 2002, Acta Astron., 52, 397
 Rogers, F. & Iglesias, C.A., 1992, ApJs, 79, 507
 Rotta, J.C., 1951, Z.Phys., 129, 547
 Schultheis, M., Glass, I.S. & Coini, M.-R., 2004, A&A, 427, 945
 Soszyński, I., Udalski, A., Kubiak, M., et al., 2004, AcA, 54, 129
 Soszyński, I., Udalski, A., Kubiak, M., et al., 2005, AcA, 55, 331
 Wood, P.R., Alcock, C., Allsmar, R.A., et al., IAU Symp. 191, Asymptotic Giant Branch Stars, ed. T. Le Bertre, A. Lébre and C. Waelkens (San Francisco: APS), 151
 Wood, P.R., 2000a, PASA, 17, 18
 Woźniak, P.R., Williams, S.J., Vestrand, W.T. & Gupta, V., 2004, AJ, 128, 2965
 Wray, J.J., Eyer, L. & Paczyński, 2004, MNRAS, 349, 1059
 Xiong, D.R., 1977, Acta Astron Sinica, 18, 86
 Xiong, D.R., 1989a, A&A, 209, 126
 Xiong, D.R., 1989b, A&A, 213, 176
 Xiong, D.R., Cheng, Q.L. & Deng, L., 1998, ApJ, 500, 449
 Xiong, D.R., Cheng, Q.L. & Deng, 2000, MNRAS, 319, 1079
 Xiong, D.R., Deng, L. & Cheng, Q.L., 1998, ApJ, 499, 355
 Xiong, D.R. & Deng, L., 2001a, MNRAS, 324, 243
 Xiong, D.R. & Deng, L., 2001b, MNRAS, 327, 1137
 Xiong, D.R. & Deng, L., 2006a, AcASn, 47, 256
 Xiong, D.R. & Deng, L., 2006b, ChA&A, 30, 379
 Yao, B.A. & Qin, D., 1993, IBVS, No.3920
 Yao, B.A., Zhang, C.S., Qin, D., 1993, IBVS, No.3955

APPENDIX A: THE INTEGRATED WORK

Using the eq. 2 in the text, its linear pulsation equations can be give as,

$$4\pi r^3 \frac{d}{dM_r} (\delta P + \delta P_t) + \frac{d}{dM_r} \left\{ 4\pi r^3 \rho \Pi^{11} \left[\frac{\delta \Pi^{11}}{\Pi^{11}} - \frac{d}{d \ln r} \left(\frac{\delta r}{r} \right) \right] \right\} - \left[r^2 \omega^2 + 4 \frac{GM_r}{r} + \frac{d}{dM_r} (4\pi r^3 \rho \Pi^{11}) \right] \frac{\delta r}{r} = 0, \quad (\text{A1})$$

where $P_t = \rho \chi^2$ is the turbulent pressure, ω is the complex frequency of oscillations defined as,

$$\omega = \omega_r + i\omega_i, \quad (\text{A2})$$

putting (A2) into (A1), solving the equation for ω , we have,

$$r^2 (\omega_r^2 + 2i\omega_i \omega_r - \omega_i^2) \frac{\delta r}{r} = 4\pi r^3 \frac{d}{dM_r} (\delta P + \delta P_t) + \frac{d}{dM_r} \left\{ 4\pi r^3 \rho \Pi^{11} \left[\frac{\delta \Pi^{11}}{\Pi^{11}} - \frac{d}{d \ln r} \left(\frac{\delta r}{r} \right) \right] \right\} - \left[4 \frac{GM_r}{r} + 3 \frac{d}{dM_r} (4\pi r^3 \rho \Pi^{11}) \right] \frac{\delta r}{r}, \quad (\text{A3})$$

The next step is multiplying eq. (A3) with $\pi (\delta r^*/r) dM_r$, then integrating it for dM_r from the center to the surface. Baring in mind that the relative pulsational amplitude at the center is zero and the pressure and density vanish at the surface, and Separating the real and imaginary parts, we have,

$$2\pi \omega_r^2 \frac{\omega_i}{\omega_r} \int_0^{M_0} \delta r \delta r^* dM_r = 4\pi^2 \int_0^{M_0} I_m \left\{ r^3 \frac{d}{dM_r} (\delta P + \delta P_t) + \frac{d}{dM_r} \left[\rho r^3 \Pi^{11} \left(\frac{\delta \Pi^{11}}{\Pi^{11}} - \frac{d}{d \ln r} \left(\frac{\delta r}{r} \right) \right) \right] \right\} \frac{\delta r^*}{r} dM_r = \pi \int_0^{M_0} I_m \left[(\delta P + \delta P_t) \frac{\delta \rho^*}{\rho} - \delta \Pi^{11} \frac{d}{d \ln r} \left(\frac{\delta r^*}{r} \right) \right] dM_r, \quad (\text{A4})$$

where I_m means to take the imaginary of the term in the brackets. $-2\pi \omega_i / \omega_r$ is the amplitude growth rate of oscillation within a cycle η ,

$$\eta = -2\pi \frac{\omega_i}{\omega_r} = -\frac{\pi}{E_k} \int_0^{M_0} I_m \left\{ (\delta P + \delta P_t) \frac{\delta \rho^*}{\rho} - \delta \Pi^{11} \frac{d}{d \ln r} \left(\frac{\delta r^*}{r} \right) \right\} dM_r. \quad (\text{A5})$$

where

$$E_k = \omega_r^2 \int \delta r \delta r^* dM_r. \quad (\text{A6})$$

As from eq. (A5), η can be divided into a gas pressure component and a Renold's stress component. We can define the IWs as functions of depth, $W_P(M_r)$ and $W_{dyn}(M_r)$, to describe the contributions of the two components,

$$W_P(M_r) = -\frac{\pi}{E_k} \int_0^{M_r} I_m \left\{ \delta P \delta \rho^* / \rho^2 \right\} dM_r, \quad (\text{A7})$$

$$W_{dyn}(M_r) = -\frac{\pi}{E_k} \int_0^{M_r} I_m \left\{ \frac{1}{\rho^2} \delta P_t \delta \rho^* - \delta \Pi^{11} \frac{d}{d \ln r} \left(\frac{\delta r^*}{r} \right) \right\} dM_r, \quad (\text{A8})$$

The gas component of the IW, $W_P(M_r)$, contains both the contribution of radiative energy transfer and the convective one. Starting from the energy equation in the text, eq. 3, we can have,

$$\delta P = (\Gamma_1 - 1) \rho \left\{ \chi^2 \left(\frac{\delta \rho}{\rho} - 3 \frac{\delta \chi}{\chi} \right) + \frac{1}{i\omega} \left[\delta \epsilon_1 - \frac{d}{dM_r} (\delta L_r + \delta L_c + \delta L_t) \right] \right\}, \quad (\text{A9})$$

where L_r , L_c and L_t are the luminosities corresponding respectively to the radiative, the convective and turbulent energy fluxes. ϵ_1 is the nuclear energy generation rate (with that of neutrino subtracted). Due to the fact that oscillations drops off abruptly towards stellar center for giant stars, the calculation of oscillating stellar model can be simplified by doing the job only for the models of envelope. Under such a condition, the contribution of energy generation rate can be safely neglected. Putting eq. (A9) into eq. (A7), the contribution of radiative energy transfer can be singled out from that of convective energy transfer,

$$W_P(M_r) = W_{Pr}(M_r) + W_{therm}(M_r), \quad (\text{A10})$$

where,

$$W_{Pr}(M_r) = -\frac{\pi}{E_k} \int_0^{M_0} Re \left\{ \frac{\Gamma_3 - 1}{\omega} \frac{\delta \rho^*}{\rho} \frac{d(\delta L_r)}{dM_r} \right\} dM_r, \quad (\text{A11})$$

$$W_{therm}(M_r) = \frac{\pi}{E_k} \int_0^{M_0} \left\{ I_m \left[3(\Gamma_3 - 1) \chi^2 \frac{\delta \rho^*}{\rho} \frac{\delta \chi}{\chi} \right] - Re \left[\frac{(\Gamma_3 - 1) \delta \rho^*}{\omega \rho} \frac{d(\delta L_c + \delta L_t)}{dM_r} \right] \right\} dM_r, \quad (\text{A12})$$

Re means taking the real part of the terms in the brackets.

W_{Pr} is the contribution of radiative energy transfer, while W_{therm} is that of convective energy transfer, i.e. the thermodynamic coupling between convection and oscillations. W_{dyn} is that due to Renold's stress, the dynamic coupling between convection and oscillations. The second and the third terms in the dynamic equations (5) and (8) for turbulent Renold stress in the text, represent the turbulent viscosity. Solving for δP_t and $\delta \Pi^{11}$ from the linear pulsation equations of eqs. (5) and (8), it is not difficult to isolate the viscosity term which is then put in eq. (A8), and we can have the turbulence viscosity component of the IW,

$$W_{vis}(M_r) = -\frac{\pi}{E_k} \int_0^{M_0} I_m \left\{ \frac{i\omega\tau_c}{\frac{4}{3} + i\omega\tau_c} \left[\chi^2 \frac{\delta \rho}{\rho} \right. \right.$$

$$\left. + \Pi^{11} \left(\frac{\delta \rho}{\rho} + 3 \frac{\delta r}{r} \right) \right] \frac{\delta \rho^*}{\rho} + \frac{4}{3} \frac{i\omega\tau_{c1}}{1 + i\omega\tau_{c1}} \left[\chi^2 \frac{d}{d \ln r} \left(\frac{\delta r}{r} \right) + \Pi^{11} \left(\frac{d}{d \ln r} \left(\frac{\delta r}{r} \right) + \frac{3}{2} \frac{\delta r}{r} \right) \right] \frac{d}{d \ln r} \frac{\delta r^*}{r} \left. \right\} dM_r$$

$$= -\frac{\pi}{E_r} \int_0^{M_0} \left\{ \frac{4}{3} (\chi^2 + \Pi^{11}) \left[\frac{\omega\tau_c}{\frac{16}{9} + \omega^2\tau_c^2} \frac{\delta \rho}{\rho} \frac{\rho^*}{\rho} + \frac{\omega\tau_{c1}}{1 + \omega^2\tau_{c1}^2} \frac{d}{d \ln r} \left(\frac{\delta r}{r} \right) \frac{d}{d \ln r} \left(\frac{\delta r^*}{r} \right) \right] \right.$$

$$\left. + \frac{\omega\tau_{c1}}{1 + i\omega^2\tau_{c1}^2} \Pi^{11} \frac{d}{d \ln r} \left(\frac{\delta r}{r} \frac{\delta r^*}{r} \right) + Re \left[\frac{3\omega\tau_c \Pi^{11}}{\frac{4}{3} + i\omega\tau_c} \frac{\delta r}{r} \frac{\delta \rho^*}{\rho} \right] \right\} dM_r, \quad (\text{A13})$$

where τ_c is the dissipation time scale of turbulence, which is also the inertia time scale of turbulence, expressed as,

$$\tau_c = \frac{c_1 r^2 P}{0.78 G M_r \rho \chi}, \quad (\text{A14})$$

$$\tau_{c1} = \frac{3}{4(1 + c_3)} \tau_c. \quad (\text{A15})$$

Subtracting eq. (A8) with eq. (A13), one has the turbulent pressure component of the IW, W_{Pt} ,

$$W_{Pt}(M_r) = W_{dyn}(M_r) - W_{vis}(M_r). \quad (\text{A16})$$

Summing up the four components, W_{Pr} , W_{therm} , W_{Pt} and W_{vis} , we have the total IW,

$$W_{all}(M_r) = W_{Pr}(M_r) + W_{therm}(M_r) + W_{Pt}(M_r) + W_{vis}(M_r), \quad (\text{A17})$$

On the right hand side of eq. (A17), only the first term is the contribution of radiative energy transfer, all the other 3 terms are due to convection, where W_{therm} is the contribution of the thermodynamic coupling between convection and oscillations, W_{Pt} is that due to turbulent pressure, and W_{vis} is that of turbulent viscosity. Under such definitions, the linear amplitude growth rate of oscillations, η , will equal the surface value of $W_{all}(M_r)$,

$$\eta = -2\pi\omega_i/\omega_r = W_{all}(M_0). \quad (\text{A18})$$

It is clear from eq. (A13) that the turbulent viscosity component W_{vis} of the IW is always negative, therefore it is a dumping against oscillations. While the effects of the turbulent pressure component W_{Pt} and turbulent thermal convection component W_{therm} depend very much on the phase of the variations of turbulent pressure P_t and turbulent thermal convection $L_c = 4\pi r^2 \rho c_P TV$ relative to that of stellar oscillations ($\delta \rho/\rho$, or $\delta r/r$). It follows from the dynamic equations of turbulent convection (eqs. 1-5) that, in general, the relative variations of convection quantities $\delta \chi/\chi$, $\delta Z/Z$, $\delta V/V$ and $\delta \Pi^{11}/\Pi^{11}$ always lag behind density variation $\delta \rho/\rho$ (or $-\delta r/r$) inside a convective zone. Under local convection approximations, this argument was proved analytically in our previous work (Xiong 1977). More general oscillation calculations using non-local convection treatment further proved this statement (Xiong, Cheng & Deng 1998, Xiong, Deng & Cheng 1998). Therefore one can conclude

from eqs. (A8 & A12) that $W_{Pt} > 0$ and $W_{therm} < 0$ general hold inside a convective zone, i.e. turbulent pressure is a excitation mechanism for oscillations, while turbulent thermal convection (the thermodynamic coupling between convection and oscillations) is a damping one. Such a theoretical analysis agrees perfectly with what have been shown in figures 7–9 for W_{Pt} , W_{therm} and W_{vis} .